Biointerface Research in Applied Chemistry
Open-Access Journal (ISSN: 2069-5837)

Article
Volume 16, Issue 1, 2026, 3
https://doi.org/10.33263/BRIAC161.003

Exploring Promising Therapeutics of Flavonoids From *Psoralea corylifolia* Against Breast Cancer through Computational Approaches

Hung Duc Nguyen [1,*]

[1] Faculty of Biology, Thai Nguyen University of Education, 24000 Thai Nguyen, Viet Nam
* Correspondence: hungnd@tnue.edu.vn;

Received: 21.11.2025; Accepted: 19.01.2026; Published: 15.02.2026

Abstract: Breast carcinoma stands as the most prevalent malignancy and a leading cause of oncological mortality in females globally. Plant-derived agents, particularly flavonoids, show considerable promise by inducing programmed cell death in neoplastic cells through multiple signaling pathways and by overcoming apoptosis resistance. The current examination assessed the anti-breast carcinoma potential of flavonoids extracted from *Psoralea corylifolia* L., emphasizing their affinity to Bcl-2 (PDB: 6QGG) using an exclusively in silico approach. The results indicate that psocorylin R (CPD1) may promote apoptosis via predicted Bcl-2 inhibition, with a docking affinity of -8.56 kcal/mol, exceeding Tamoxifen (-6.76 kcal/mol). Across 100 ns dynamics simulations, the CPD1-6QGG assembly demonstrated durability (RMSD 0.15-0.25 nm; Rg 1.4-1.5 nm) with sustained hydrogen bonding (0-6; average 3) and SASA oscillations of 75-90 nm². MM/GBSA analyses yielded a binding strength of -25.4 ± 6.37 kcal/mol for CPD1 versus -20.04 ± 4.42 kcal/mol for Tamoxifen, and DFT descriptors (e.g., ΔE = 2.44 eV) supported CPD1 interaction potential. Nevertheless, conclusions are limited by the absence of experimental validation, no in vitro/*in vivo* efficacy or safety assays, and by not assessing off-target effects or unintended covalent reactivity, warranting systematic experimental confirmation.

Keywords: apoptosis; Bcl-2; breast cancer; DFT; flavonoid; molecular modeling.

1. Introduction

Breast carcinoma ranks as the predominant malignancy diagnosed and the primary contributor to cancer fatalities among females worldwide. This neoplasm constitutes roughly one-quarter of novel oncological incidences in females globally, while topping mortality rates, with projections of 670,000 deaths in 2022 [1,2]. Recent investigative endeavors have substantially enhanced the comprehension and management of breast carcinoma, with key advancements in personalized medicine, refined screening technologies, targeted therapies, and novel approaches to risk stratification [3,4].

Apoptosis is programmed cell death, a natural process that is crucial for normal development but is disrupted in breast cancer, allowing abnormal cells to proliferate. Cancer cells often evade apoptosis, making their induction a key goal for breast cancer treatments like chemotherapy and radiation. Researchers are also developing strategies to directly promote apoptosis in cancer cells by targeting the proteins and pathways involved [5,6]. Breast cancer

cells evade cell death through a combination of mechanisms, including manipulating signaling pathways, overexpressing anti-apoptotic proteins such as Bcl-2 and Mcl-1 to prevent programmed cell death, and increasing the expression of genes that promote cell survival. These strategies allow cancer cells to resist therapies and continue to proliferate [7-9].

Plant-derived compounds are a significant source of modern cancer treatments, with several clinically approved chemotherapy drugs originating from plant extracts or their semi-synthetic derivatives. These compounds act through various mechanisms to target and inhibit cancer cell growth, often with lower toxicity to healthy tissues than some conventional treatments [10-12]. Flavonoids, a class of natural plant-based compounds found in fruits, vegetables, and teas, show significant anticancer properties through various mechanisms. Extensive in vitro and *in vivo* studies suggest that a diet rich in flavonoids may help reduce cancer risk and enhance the effectiveness of conventional cancer therapies [13]. *Psoralea corylifolia* L., or "Bu-gu-zhi," is a significant medicinal herb in Traditional Chinese Medicine, valued for warming kidneys, strengthening bones, and treating issues like vitiligo, kidney-yang deficiency, and back pain, thanks to its rich content of coumarins, flavonoids, and other compounds with antibacterial, anti-inflammatory, and antioxidant properties. Previous studies by our colleagues have identified two flavonoids from P. corylifolia with significant cytotoxicity against the MCF-7 breast cancer cell line via the Bcl-2/Bax/cleaved caspase-3 axis, providing a direct mechanistic rationale for prioritizing this phytochemical space and targeting Bcl-2; however, their mechanisms remain unexplored [14]. This led us to conduct this study to discover and evaluate the mechanisms of these flavonoids using multiple computational techniques. Molecular docking, molecular dynamics simulation, MMGBSA, and DFT calculation were carried out. The study findings establish a foundation for subsequent experimental validation and refinement of these flavonoids as promising, effective, low-toxicity therapeutics for breast cancer, contingent on further in vitro and *in vivo* investigations.

2. Materials and Methods

2.1. Structural preparation of selected ligands.

The selected flavonoids, including psocorylin R (CPD1) and psocorylin S (CPD2), have molecular formulas of $C_{40}H_{40}O_8$ and $C_{40}H_{38}O_9$, respectively, with molecular weights of 648.2723 and 662.2516 *m/z*. The Tamoxifen, possessing a molecular formula of $C_{26}H_{29}NO$ and a molecular weight of 371.2249 *m/z*, was chosen as the comparative reference (Figure 1).

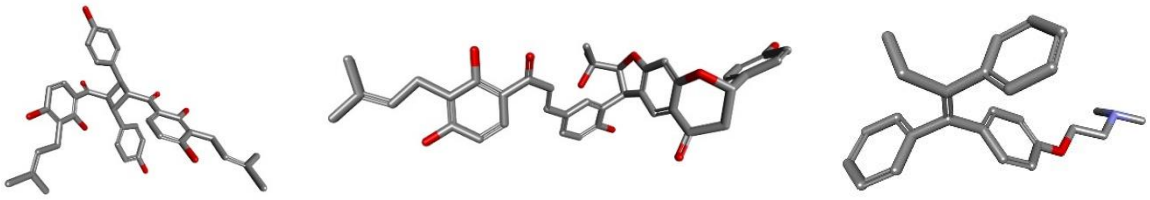

(a) **(b)** **(c)**

Figure 1. 3D Structures of selected ligands. (**a**) CPD1; (**b**) CPD2; (**c**) Tamoxifen.

2.2. Molecular docking.

Generation of three-dimensional structures for selected ligands proceeded in PDB format using Biovia Discovery Studio Visualizer, which incorporates polar hydrogens, computes Gasteiger charges, and enables flexibility across torsional bonds. Acquisition of the

Bcl-2 protein structure (PDB ID: 6QGG) in PDB format occurred from the RCSB Protein Data Bank [15]. Docking simulations between ligands and proteins were performed using AutoDock Tools, employing a grid box of 60 points per x, y, and z dimension with a spacing of 0.375 Å. Binding site coordinates on the 6QGG structure received assignments of x = -13.963 Å, y = 13.180 Å, and z = -4.218 Å. This grid definition was selected to (i) fully encompass the Bcl-2 binding region of interest (including residues capable of interacting with diverse ligand chemotypes) and (ii) provide sufficient space for complete ligand translation/rotation while maintaining a practical computational cost; in AutoDock, the grid box is expected to include all atoms potentially contributing to intermolecular interactions and be large enough to allow free ligand movement. Regarding the force-field/scoring choice, AutoDock4 employs a semi-empirical free-energy-based scoring function, combined with partial-charge assignment, to estimate binding free energy and rank poses. The implementation of the Lamarckian genetic algorithm facilitated the identification of minimal-energy conformations that enhanced interaction stability. Following simulation completion, the conformation with the superior binding affinity was evaluated in Discovery Studio Client 2024 and compared with Tamoxifen docking results on the equivalent protein to determine relative affinity traits [16].

2.3. Molecular dynamics simulation.

Molecular dynamics simulations occurred for the superior docked conformation associated with the 6QGG protein across a 100 ns duration, utilizing GROMACS software version 2024.4 [17]. Refinement of the protein configuration addressed missing atoms and residues via Swiss-PdbViewer [18]. Generation of ligand topologies employed SwissParam [19]. Solvation involved enclosing the protein-ligand complex in a triclinic container, using the SPC water model supplemented with 0.15 M sodium chloride. Structural optimization and neutralization were achieved through 50,000 steps of energy minimization. Equilibration encompassed a 200 ps NVT ensemble succeeded by a 200 ps NPT ensemble, maintained at 300 K and 1.0 bar, employing the V-rescale thermostat and Parrinello–Rahman barostat. Execution of three independent 100 ns productions incorporated a 2 fs time step, PME electrostatics, a 1.2 nm real-space cutoff for Coulomb and van der Waals interactions, and LINCS constraints on bonds involving hydrogen. Three independent 100 ns trajectories were generated for each complex. Coordinates and energies were recorded every 10 ps. Processing of simulation outputs through the Grace software yielded essential parameters, including root mean square deviation (RMSD), residue-specific root mean square fluctuation (RMSF), radius of gyration (Rg), number of hydrogen bonds (H-bonds), and solvent-accessible surface area (SASA). Assessment of conformational stability in complexes utilized UCSF Chimera version 1.13.3 for alignments [20]. The superposition of ligand orientations at 0 ns and 100 ns onto the protein active site allowed for the evaluation of persistent interactions with essential residues, including hydrogen bonds, van der Waals forces, and hydrophobic contacts, throughout the simulation. Such an approach facilitated a comprehensive understanding of the interaction dynamics and endurance between ligands and the protein during the 100 ns interval.

2.4. Molecular mechanics generalised Born surface area (MMGBSA) analysis.

MMGBSA computations were performed using the gmx_MMPBSA utility, with the CHARMM36 force field, to assess binding free energies for the CPD1-6QGG and Tamoxifen-6QGG complexes. Electrostatic solvation contributions received treatment via the generalized

Born model in an implicit solvent framework, while non-polar solvation terms arose from solvent-accessible surface area evaluations. The derivation of these energies was based on molecular dynamics trajectories, which employed 125 uniformly distributed frames sampled at 80 ps intervals over an 80 ns segment (from 20 ns to 100 ns). Averaging of outcomes delineated variability in ligand-protein interactions, elucidating affinity strength and structural stability within the simulated context.

2.5. Quantum chemistry computation using the density functional theory (DFT) method.

Optimization of molecular geometries for CPD1 and Tamoxifen proceeded via the ORCA 6.1.0 quantum chemistry software [21]. Construction of preliminary molecular frameworks was performed in Avogadro [22], with subsequent visualization and orbital analysis in IboView version 20211019 [23]. Geometry optimization was carried out at the MP2/def2-SVP level of theory. Geometry optimizations were considered converged when the maximum/RMS gradients and maximum/RMS displacements, as well as the energy change between optimization cycles, satisfied the default ORCA 6.1!Opt convergence thresholds (TolE = 5×10^{-6} a.u., TolMaxG = 3×10^{-4} a.u., TolRMSG = 1×10^{-4} a.u., TolMaxD = 4×10^{-3} a.u., TolRMSD = 2×10^{-3} a.u.). SCF convergence was required at every optimization step, and only calculations reporting “SCF CONVERGED” and final “OPTIMIZATION CONVERGED” in the ORCA output were used for subsequent descriptor analysis. Extraction from optimized configurations included quantum descriptors like HOMO and LUMO energies, energy gap (ΔE), chemical potential (μ), electronegativity (χ), hardness (η), softness (σ), and electrophilicity index (ω). Application of Koopmans’ theorem facilitated the approximation of these metrics to delineate electronic attributes and reactivity tendencies of the molecules [24,25]. These global descriptors were selected because they provide a compact electronic-structure rationale for noncovalent recognition in biological environments, which can influence hydrogen bonding, electrostatic complementarity, and π-interactions with protein residues. Accordingly, the descriptors are used here to support mechanistic interpretation of ligand-biomolecule interaction tendencies rather than to infer *in vivo* anticancer efficacy directly.

3. Results and Discussion

3.1. Molecular docking analysis.

Molecular docking is an *in silico* method used to predict the binding pose of a ligand within a protein's binding site, i.e., its orientation and conformation. The goal is to identify the most favorable binding mode, which can be ranked by a scoring function that estimates the binding affinity. Evaluation of binding affinities and intermolecular associations was performed for selected compounds with the Bcl-2 protein (PDB ID: 6QGG), using Tamoxifen as a comparative reference. The presentation of compound interactions at the binding pockets on 6QGG, as shown in Table 1, emphasizes the participating amino acids and locations in the ligand contact region. Molecular docking revealed principal non-covalent mechanisms, encompassing hydrogen bonds, van der Waals forces, and hydrophobic interactions between the protein and the selected ligands.

Table 1. The interactions between the docked ligands and the protein 6QGG.

Docked ligands	Binding energy (kcal/mol)	Hydrogen bond	Van der Waals force	Hydrophobic interaction
CPD1	-8.56	Asn143, Gly145, Arg146	Gln99, Asp103, Arg107, Leu137, Trp144, Phe198	Ala100, Phe104, Tyr108, Arg146, Val148, Ala149, Leu201, Tyr202
CPD2	-8.47	Arg107, Tyr108, Arg139, Asp140, Asn143, Gly145, Arg146, Leu201	Thr99, Gln99, Asp103, Phe104, Glu136, Leu137, Ala149	Ala100, Gly145, Arg146, Tyr202
Tamoxifen	-6.76	Ala149, Glu152	Ser105, Asp111, Phe112, Met115, Val133, Glu136, Gly145, Phe153, Val156	Phe104, Tyr108, Leu137, Arg146, Ala149

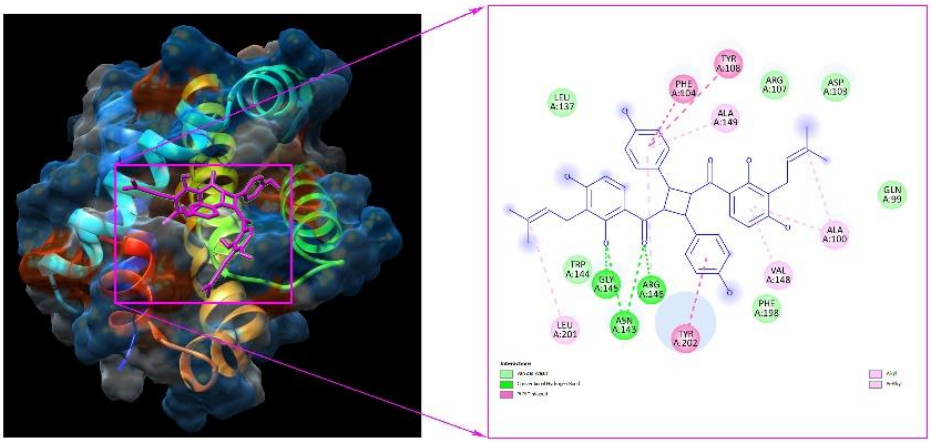

(a)

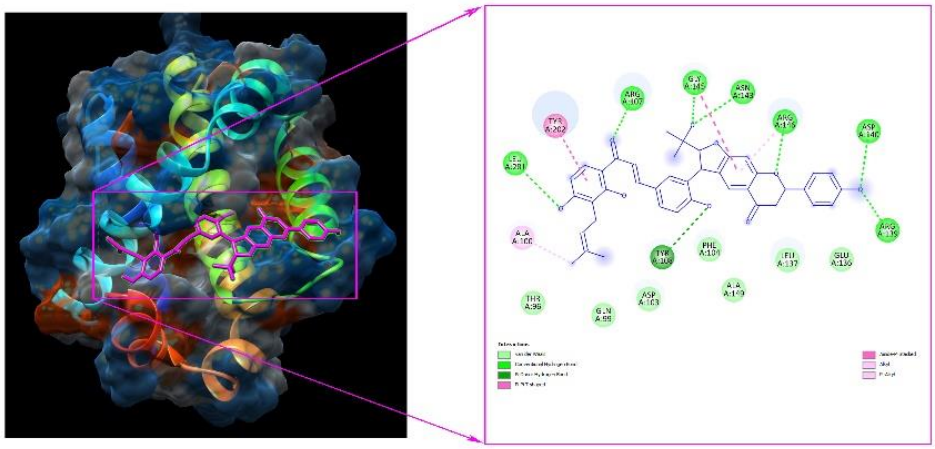

(b)

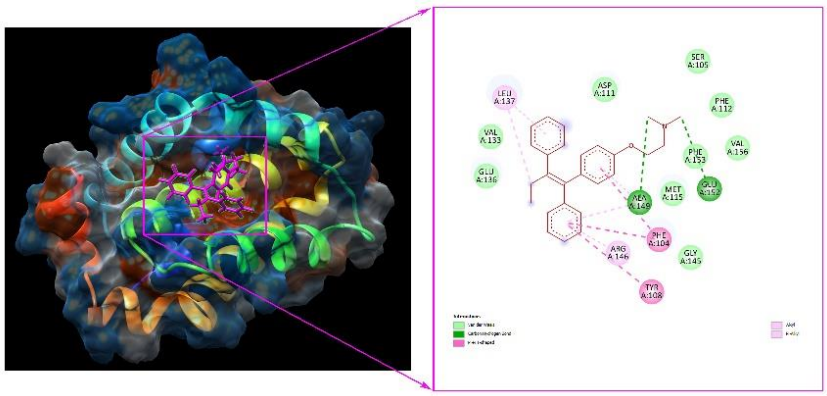

(c)

Figure 2. Molecular docking model and 2D interaction diagram of **(a)** CPD1; **(b)** CPD2; **(c)** Tamoxifen with 6QGG protein.

Compounds CPD1 and CPD2 exhibited specific interactions with the Bcl-2 protein, which is essential for regulating apoptosis in cancer-related processes. CPD1 displayed engagement through 11 active site residues (Ala100, Asp103, Phe104, Tyr108, Leu137, Trp144, Gly145, Val148, Ala149, Phe198, Tyr202) and formed hydrogen bonds with Asn143, Gly145, Arg146. The binding energy for the CPD1-6QGG complex is registered at -8.56 kcal/mol (Figure 2a).

CPD2, in comparison, interacted via 8 active site residues (Ala100, Asp103, Phe104, Tyr108, Leu137, Gly145, Ala149, Tyr202) and established hydrogen bonds involving Arg107, Tyr108, Arg139, Asp140, Asn143, Gly145, Arg146, Leu201. This configuration yielded a binding energy of -8.47 kcal/mol for CPD2-6QGG assembly, indicating a stable conformation (Figure 2b).

Tamoxifen, as a reference ligand, engaged 7 active site residues (Phe104, Tyr108, Asp111, Met115, Leu137, Gly145, Ala149) and created hydrogen bonds with Ala149 and Glu152. The binding energy with 6QGG reached -6.76 kcal/mol. Despite effective involvement, Tamoxifen showed reduced affinity and fewer engagements than CPD1, suggesting diminished binding capacity relative to the superior compound (Figure 2c).

Although CPD1 and CPD2 showed more favorable predicted binding energies than Tamoxifen, the biological significance of relatively small docking-score differences should be interpreted cautiously. The docking binding energy reported by AutoDock is an approximate scoring estimate rather than an experimentally measured free energy; therefore, differences on the order of 1-2 kcal/mol may fall within the intrinsic uncertainty of the scoring function and the sampling protocol. In thermodynamic terms, if a docking score of 1.8 kcal/mol were fully real, it would correspond to an estimated 15-25-fold difference in equilibrium affinity at room/physiological temperature. However, because docking energies are model-dependent and may not translate directly into potency, the observed 1.8 kcal/mol gap between CPD1 and Tamoxifen should be viewed as a trend suggesting potentially improved affinity, not definitive proof of superior biological activity.

Docking assessments against Bcl-2 identified diverse non-covalent interactions, including hydrogen bonds, van der Waals interactions, and hydrophobic contacts, that contribute to complex stability [26]. Hydrogen bonds enable directed associations via atomic electron sharing, often with oxygen or nitrogen. Hydrophobic contacts arise from the clustering of nonpolar segments in aqueous environments, thereby minimizing solvent interactions and promoting compact structures. Van der Waals forces supplement these by promoting proximity alignments that amplify collective efficiency. Greater negativity in binding energies generally indicates greater durability and prolonged ligand occupancy at binding sites [27].

The selection of CPD1 for subsequent molecular dynamics analysis was based on its prominent docking performance with the 6QGG protein, characterized by the most favorable binding energy of -8.56 kcal/mol and substantial active-site participation via 11 residues, including hydrogen bonds. This surpassed CPD2 (-8.47 kcal/mol) and Tamoxifen (-6.76 kcal/mol), positioning CPD1 as a prime candidate for investigating sustained stability and interaction persistence within the Bcl-2 domain. Emphasis on CPD1 supports a detailed exploration of conformational shifts, energy distributions, and residue contributions over simulation periods, with Tamoxifen serving as a comparative reference for evaluating apoptosis modulation in oncology approaches. Accordingly, the prioritization of CPD1 for downstream molecular dynamics was not based solely on a modest improvement in docking score (docking score = 1.8 kcal/mol versus Tamoxifen), because docking energies are

approximate and small differences can fall within the scoring function's uncertainty. Instead, CPD1 was selected based on qualitative binding features: it established a more coherent interaction network within the Bcl-2 groove, combining extensive hydrophobic packing with multiple hydrogen-bond contacts to pocket residues, and exhibited broader residue engagement than the reference ligand. Molecular dynamics was therefore employed as a necessary follow-up to test whether the predicted pose remains stable over time and whether these interactions persist under a dynamic, solvated environment, providing stronger evidence for potential biological relevance beyond docking scores alone.

3.2. Molecular dynamics simulation.

Molecular dynamics simulation is a powerful method for modeling protein conformational changes by simulating atomic motion over time according to physical principles. The combination of molecular docking and molecular dynamics simulation is a crucial tool in drug discovery, as docking identifies potential drug candidates by predicting their binding poses and affinities. In contrast, molecular dynamics simulates the stability and conformational changes of that complex over time. This synergy provides a more complete understanding of how a potential drug interacts with its target, allowing researchers to optimize lead compounds more efficiently. Therefore, the evaluation systematically investigated RMSD, RMSF, Rg, hydrogen bond formation, and SASA metrics to determine the stability, flexibility, and solvent exposure of the CPD1-6QGG and Tamoxifen-6QGG complexes throughout the simulation timeframe. Consequently, the total energy and potential energy values for the CPD1-6QGG complex were found to be -209,610 kJ/mol and -261,032 kJ/mol, respectively. For the Tamoxifen-6QGG complex, the total energy and potential energy values were measured to be -210,129 kJ/mol and -261,597 kJ/mol, respectively. The simulation system maintained equilibrium at a temperature of 300 K.

The RMSD is a measure of the average distance between the atoms of two superimposed molecular structures, used in both molecular dynamics and docking to assess structural similarity and accuracy. In dynamics, it tracks how much a molecule's structure changes over time, with a low or stable RMSD indicating stability. Throughout the 100 ns simulation, RMSD trajectories for the CPD1-6QGG and Tamoxifen-6QGG complexes showed comparable patterns. The CPD1-6QGG configuration exhibits RMSD measures ranging from 0.15 to 0.25 nm, with an average of approximately 0.20 nm, indicating notable structural stability and robust accommodation in the 6QGG binding site. Similarly, the Tamoxifen-6QGG association showed RMSD values between 0.15 and 0.25 nm, with a mean near 0.20 nm, indicating balanced flexibility and maintained architectural integrity (Figure 3a). Such parallels emphasize spatial consistency across both pairings, potentially stemming from analogous anchoring in the target region. In summary, RMSD evaluations indicate that CPD1-6QGG and Tamoxifen-6QGG preserve their reference conformations with similar fidelity in the conducted analyses.

Calculating the RMSF for each residue in protein-ligand complexes to measure and understand how much each residue moves or fluctuates during a simulation, which reveals the flexibility of the complex at a residue level. High RMSF values indicate a residue is more flexible, while low RMSF values suggest rigidity and structural stability. As illustrated in Figure 3b, RMSF values for CPD1-6QGG and Tamoxifen-6QGG complexes, emphasizing residues Ser8 to Gly203, range predominantly from 0.05 to 0.2 nm. The CPD1-6QGG setup

maintains RMSF near 0.1 nm throughout much of this interval, indicating curtailed oscillations and enhanced framework durability, which may influence interactions at critical locations.

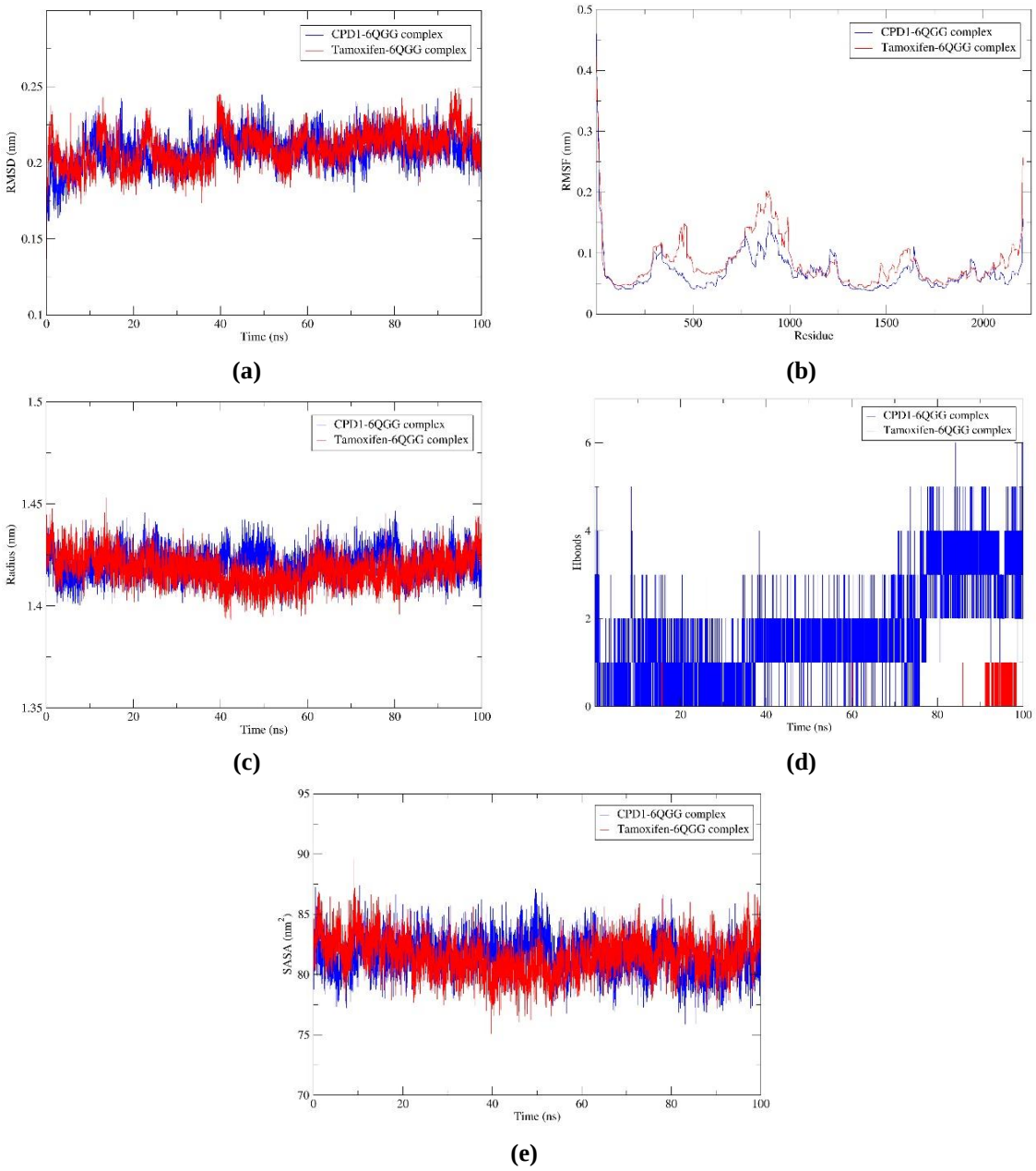

Figure 3. Results of MD simulation for the bindings of CPD1 (blue) and Tamoxifen (red) with 6QGG protein. **(a)** RMSD; **(b)** RMSF; **(c)** Rg; **(d)** Hbonds; **(e)** SASA.

The Tamoxifen-6QGG configuration aligns closely, averaging around 0.1 nm with intermittent congruences and slight reductions, denoting parallel degrees of confinement. Such uniformity between the two arrangements accentuates the ligands' function in consolidating the protein, consequently enhancing commitments within active regions.

Analyzing the Rg over time helps researchers study conformational changes, stability, and flexibility of proteins and other large molecules. A lower Rg value indicates a more compact, tightly-folded structure, while a higher value suggests a more extended, flexible, and less compact structure. As shown in Figure 3c, the Rg values for the CPD1-6QGG and Tamoxifen-6QGG complexes emerge over 100 ns. Both reveal stable variations between 1.4 and 1.5 nm, averaging approximately 1.45 nm, indicating a persistent ordered arrangement of the 6QGG protein under bound conditions throughout the whole simulation.

In molecular dynamics, the number of hydrogen bonds is a measure of inter- and intramolecular interactions, system stability, and phase-change properties. A higher number can indicate stronger interactions and a more stable system, while changes in the number, particularly with temperature, can signify melting or other phase transitions. During the 100 ns simulation, the CPD1-6QGG complex varied from 0 to 6 bonds, contrasting with the Tamoxifen-6QGG span of 0 to 2 bonds (Figure 3d). This persistent interaction indicates a secure positioning within the 6QGG protein's binding site over the duration, with the CPD1-6QGG complex typically maintaining approximately 3 bonds on average, surpassing the roughly 1 bond maintained by the Tamoxifen-6QGG complex. This disparity underscores CPD1's advantage in forming stronger interactions with the 6QGG protein.

The SASA quantifies the molecular surface exposed to solvent, providing insights into structural dynamics, folding processes, and binding events. Computation involves tracing a probe sphere, mimicking solvent, across the van der Waals envelope. Monitoring SASA evolution during simulations facilitates the deciphering of molecular responses, including protein reconfiguration and ligand association with targets. Here, SASA trajectories for CPD1-6QGG and Tamoxifen-6QGG complexes underwent examination to assess alterations in solvent exposure. Over the 100 ns interval, both exhibited sustained oscillations, spanning roughly 75 to 90 nm^2, with an average of approximately 82 nm^2. Such variations suggest subtle shifts in solvent-protein interfaces, prompted by ligands, which may influence the persistence of attachment. Comparable ranges and averages across both configurations indicate balanced solvent interactions, reflecting robust accommodation in the 6QGG cavity despite ligand differences.

Overall, RMSD and Rg profiles indicate that both CPD1-6QGG and tamoxifen-6QGG complexes remain globally stable throughout 100 ns. While these global metrics are comparable, CPD1 shows more persistent binding-site interactions, evidenced by a higher number of hydrogen bonds and consistently low residue fluctuations across the protein. Therefore, CPD1 demonstrates interaction stability comparable to, and locally stronger than, Tamoxifen, supporting its potential as an alternative ligand for 6QGG.

3.3. Free binding energy (MMGBSA) analysis.

The MMGBSA approach was used to estimate binding free energies for these ligand-protein associations, employing the gmx_MMPBSA software alongside the CHARMM36 force field. Frames from complete molecular dynamics paths, spanning an 80-ns period, underwent this analysis. The binding free energy (ΔG_bind) for each complex follows $\Delta G\_bind = G\_complex - (G\_receptor + G\_ligand)$, with G_receptor as the unbound receptor energy and G_ligand as the isolated ligand energy. Equivalently, it decomposes to $\Delta G\_bind = \Delta H - T\Delta S$, ΔH as enthalpy variation, and $-T\Delta S$ as entropy cost from association. Omitting entropy yields a comparative energy measure apt for assessing affinities in analogous setups. This review encompassed the 80 ns range, drawing 125 frames at 80 ps spacings (20 to 100 ns). Averaged energies thus obtained reflect association fluidity, offering clues to ligand effectiveness and endurance in simulated biological settings. MMGBSA outcomes for the associations feature in Table 2.

Notably, the ~5.36 kcal/mol difference between the mean ΔG_bind values should be interpreted in the context of the frame-to-frame fluctuations (SD), and is therefore discussed as a modest trend supported by consistent energetic components rather than a definitive quantitative separation. MMGBSA results support the docking trend and the MD interaction

patterns, with CPD1-6QGG showing a more favorable (more negative) ΔG_bind (-25.40 ± 6.37 kcal/mol) than tamoxifen-6QGG (-20.04 ± 4.42 kcal/mol).

Table 2. Free energy of binding obtained using MMGBSA calculations.

Energy component	Average (kcal/mol)		Standard deviation	
	CPD1-6QGG	Tamoxifen-6QGG	CPD1-6QGG	Tamoxifen-6QGG
ΔBOND	0	0	0	0
ΔANGLE	0	0	0	0
ΔDIHED	0	0	0	0
ΔUB	0	0	0	0
ΔIMP	0	0	0	0
ΔCMAP	0	0	0	0
ΔVDWAΔALS	-35.48	-32.53	3.74	5.01
ΔEEL	-29.04	-5.67	12.42	3.02
Δ1-4 VDW	0	0	0	0
Δ1-4 EEL	0	0	0	0
ΔEGB	44.14	22.56	8.63	3.97
ΔESURF	-5.01	-4.39	0.50	0.59
ΔGGAS	-64.52	-38.21	13.77	7.17
ΔGSOLV	39.13	18.17	8.36	3.51
ΔTOTAL	-25.40	-20.04	6.37	4.42

Given that the entropic contribution (-TΔS) was not included, these values are best interpreted as a comparative ranking under an identical protocol, rather than absolute binding free energies. The observed preference for CPD1 is consistent with its stronger interaction energetics, particularly the more favorable van der Waals (-35.48 vs -32.53 kcal/mol) and electrostatic terms (-29.04 vs -5.67 kcal/mol), alongside its higher hydrogen-bond persistence in MD. Meanwhile, similar global stability descriptors (RMSD, Rg, RMSF, and SASA) indicate that the difference is driven mainly by binding-site interaction energetics rather than large-scale conformational changes. Overall, within the limitations of entropy omission, MMGBSA provides additional evidence that CPD1 has a modest affinity advantage for 6QGG under the simulated conditions.

3.4. Quantum chemistry computation using the density functional theory (DFT) method.

Density functional theory (DFT) computations were performed to examine CPD1 and Tamoxifen, assessing their electronic properties and potential interaction patterns based on the listed parameters. Energies of the highest occupied molecular orbital (EHOMO) and the lowest unoccupied molecular orbital (ELUMO) provide essential information on molecular electron distributions, stability, and response properties. EHOMO value reflects propensity for electron donation, whereas ELUMO value denotes aptitude for electron reception. CPD1 presents EHOMO at -7.5102 eV, higher than Tamoxifen's -8.2085 eV, implying CPD1 exhibits greater ease in electron release and potentially lower oxidation resistance. In contrast, CPD1 exhibits a more negative ELUMO (-5.0696 eV) than Tamoxifen (+3.2069 eV). Under the adopted definition (EA = -ELUMO), this corresponds to a more positive EA for CPD1, suggesting a greater tendency to accommodate incoming electron density.

Table 3. Quantum descriptors of CPD1 and Tamoxifen.

Molecule	EHOMO (eV)	ELUMO (eV)	ΔE (eV)	μ (eV)	χ (eV)	η (eV)	σ (eV^{-1})	ω (eV)
CPD1	-7.5102	-5.0696	2.4406	-6.2899	6.2899	1.2203	0.8195	16.2103
Tamoxifen	-8.2085	3.2069	11.4154	-2.5008	2.5008	5.7077	0.1752	0.5479

EHOMO (eV): highest occupied molecular orbitals; **ELUMO (eV)**: lowest unoccupied molecular orbitals; **ΔE (eV)**: energy gap; **μ (eV)**: chemical potential; **χ (eV)**: electronegativity; **η (eV)**: hardness; **σ (eV^{-1})**: softness; **ω (eV)**: electrophilicity index.

The energy gap (ΔE), derived from ELUMO minus EHOMO, serves as an indicator of molecular rigidity and stability; narrower gaps typically associate with elevated activity and decreased rigidity, while broader gaps are associated with the opposite (Table 3, Figure 4).

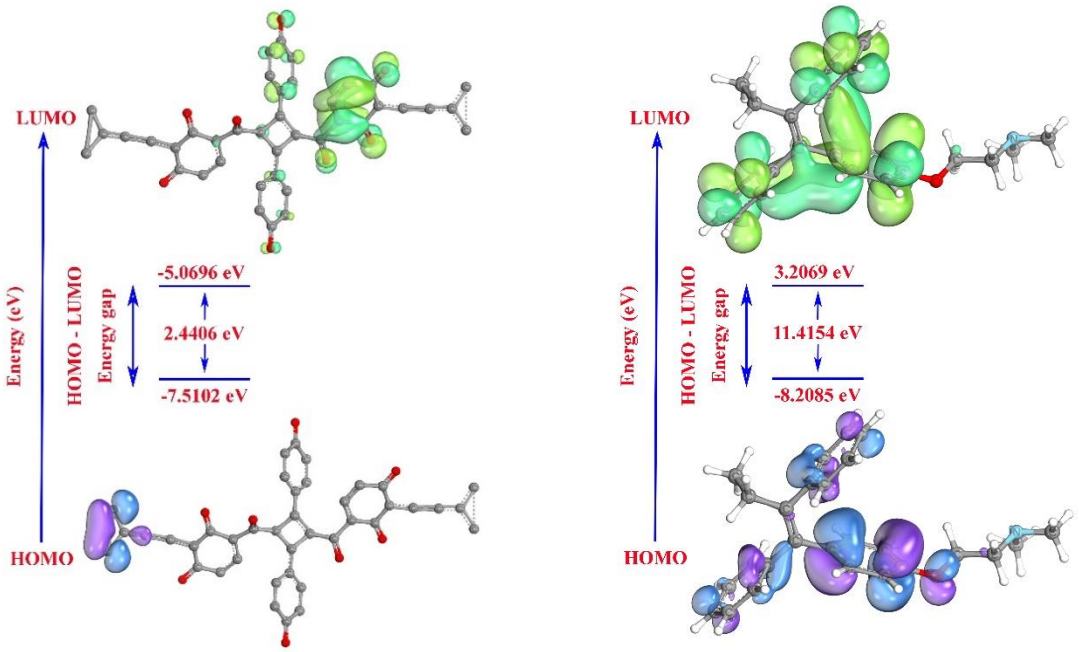

(a) **(b)**

Figure 4. HOMO and LUMO surface diagrams of **(a)** CPD1; **(b)** Tamoxifen.

With ΔE values of 2.4406 eV for CPD1 and 11.4154 eV for Tamoxifen, CPD1 shows a smaller gap, suggesting higher intrinsic electronic reactivity and lower electronic rigidity than Tamoxifen. These descriptors reflect physicochemical tendencies and are not direct predictors of *in vivo* anticancer efficacy. The ionization potential (IP), as a negative value of EHOMO, quantifies the energy required for electron detachment, with higher values indicating a robust oxidation barrier. Electron affinity (EA), as a negative ELUMO, measures the ease of electron incorporation, with more positive values indicating greater affinity. CPD1 yields IP of 7.5102 eV and EA of 5.0696 eV, against Tamoxifen's IP of 8.2085 eV and EA of -3.2069 eV, underscoring CPD1's lesser barrier to electron removal alongside superior electron gain. Tamoxifen, meanwhile, demonstrates stronger electron retention but inferior acceptance. Hardness (η), computed as ΔE/2, evaluates opposition to electron configuration alterations, and softness (σ), as 1/η, signifies adaptability in responses. CPD1 features a hardness of 1.2203 eV and a softness of 0.8195 eV^{1}, whereas Tamoxifen shows a hardness of 5.7077 eV and a softness of 0.1752 eV^{1}, revealing CPD1 as considerably less resistant to electronic modifications. Electronegativity (χ), from the average of IP and EA (χ = (IP + EA)/2), measures electron attraction in linkages. CPD1's χ at 6.2899 eV surpasses Tamoxifen's 2.5008 eV, indicating CPD1 holds more decisive influence over shared electrons. Chemical potential (μ), as negative electronegativity (μ = -χ), describes electron flow directions, with more negative levels promoting uptake. CPD1's μ of -6.2899 eV, compared to Tamoxifen's -2.5008 eV, implies that CPD1 favors electron accumulation more prominently. Finally, the electrophilicity index (ω), defined as $\omega = \mu^2/(2\eta)$, measures electrophilic strength, with higher numbers indicating stronger inclinations. CPD1's ω of 16.2103 eV considerably outstrips Tamoxifen's 0.5479 eV, proposing CPD1 engages more assertively as an electrophile with surrounding entities. Notably, these global DFT descriptors describe intrinsic electronic features (reactivity/polarizability) and can only support hypotheses on interaction tendencies. *In vivo*

anticancer efficacy is multifactorial (e.g., solubility, permeability, metabolism, distribution, and target engagement) and therefore cannot be inferred from DFT descriptors alone. Hence, DFT results are discussed here as supportive physicochemical evidence complementary to docking/biological data.

4. Conclusions

This work provides a computational evaluation of selected ligands as putative modulators of the anti-apoptotic protein Bcl-2 (PDB: 6QGG). Among the screened compounds, CPD1 showed a more favorable predicted binding affinity (-8.56 kcal/mol) than Tamoxifen (-6.76 kcal/mol), with interaction patterns consistent with stabilizing noncovalent contacts, including hydrogen bonding and van der Waals contributions. Molecular dynamics trajectories (100 ns) supported conformational stability of the CPD1-6QGG complex, characterized by RMSD values around 0.20 nm, a radius of gyration near 1.45 nm, and an average of approximately three hydrogen bonds, exceeding the corresponding hydrogen-bond count observed for Tamoxifen. MM/GBSA estimates further indicated stronger binding for CPD1 (-25.4 ± 6.37 kcal/mol) relative to Tamoxifen (-20.04 ± 4.42 kcal/mol), with notable contributions from van der Waals and electrostatic terms. Frontier-orbital descriptors and derived indices suggested distinct electronic features for CPD1 compared with Tamoxifen; however, these descriptors are best interpreted as supportive physicochemical indicators rather than direct predictors of biological efficacy.

Translational significance remains provisional because computational outputs represent hypothesis-generating evidence that depends on model assumptions and parameterization. Experimental confirmation is therefore required to determine whether CPD1 exhibits measurable Bcl-2 inhibition, target engagement, and anticancer activity under biological conditions. Priority directions include biochemical binding and functional assays, cell-based apoptosis and viability studies, selectivity profiling across the Bcl-2 family, and evaluation of pharmacokinetic and safety-relevant properties. In addition, assessment of unintended covalent reactivity is warranted to exclude nonspecific mechanisms. Subject to supportive in vitro and *in vivo* outcomes, CPD1 may represent a candidate for subsequent optimization and preclinical development.

Author Contributions

Conceptualization, H.D.N.; methodology, H.D.N.; investigation, H.D.N.; data curation, H.D.N.; formal analysis, H.D.N.; writing—original draft preparation, H.D.N.; writing—review and editing, H.D.N.; visualization, H.D.N. The author has read and agreed to the published version of the manuscript.

Institutional Review Board Statement

Not applicable.

Informed Consent Statement

Not applicable.

Data Availability Statement

Data supporting the findings of this study are available upon reasonable request from the corresponding author.

Funding

This research received no external funding.

Acknowledgments

The contributors to this work, whether directly or indirectly, have our sincere gratitude.

Conflicts of Interest

The author declares no conflict of interest.

References

1. Bray, F.; Laversanne, M.; Sung, H.; Ferlay, J.; Siegel, R.L.; Soerjomataram, I.; Jemal, A. Global cancer statistics 2022: GLOBOCAN estimates of incidence and mortality worldwide for 36 cancers in 185 countries. *CA. Cancer J. Clin.* **2024**, *74*, 229-263, https://doi.org/10.3322/caac.21834.
2. Redig, A.J.; McAllister, S.S. Breast cancer as a systemic disease: a view of metastasis. *J. Intern. Med.* **2013**, *274*, 113-126, https://doi.org/10.1111/joim.12084.
3. Roarty, K.; Echeverria, G.V. Laboratory Models for Investigating Breast Cancer Therapy Resistance and Metastasis. *Front. Oncol.* **2021**, *11*, 645698, https://doi.org/10.3389/fonc.2021.645698.
4. Mennella, C.; Maniscalco, U.; De Pietro, G.; Esposito, M. Ethical and regulatory challenges of AI technologies in healthcare: A narrative review. *Heliyon* **2024**, *10*, e26297, https://doi.org/10.1016/j.heliyon.2024.e26297.
5. Werner, H.; Oh, Y.; Roberts, C.T. Apoptosis in breast cancer. In Advances in Cell Aging and Gerontology; Elsevier: **2001**; Volume 6, pp. 1-22, https://doi.org/10.1016/S1566-3124(01)06001-1.
6. Kadam, C.Y.; Abhang, S.A. Chapter Five - Apoptosis Markers in Breast Cancer Therapy. In Advances in Clinical Chemistry, Makowski, G.S., Ed.; Elsevier: **2016**; Volume 74, pp. 143-193, https://doi.org/10.1016/bs.acc.2015.12.003.
7. Mansour, M.A.; El-Salamoni, M.A.-F.; Mostafa, H.N. Harnessing PUMA's lethal potential: BCL-2 family dynamics and novel strategies to combat cancer recurrence. *Cancer Treat. Res. Commun.* **2025**, *44*, 100975, https://doi.org/10.1016/j.ctarc.2025.100975.
8. Williams, M.M.; Cook, R.S. Bcl-2 family proteins in breast development and cancer: could Mcl-1 targeting overcome therapeutic resistance?. *Oncotarget* **2015**, *6*, 3519-3530, https://doi.org/10.18632/oncotarget.2792.
9. Shenoy, T.N.; Abdul Salam, A.A. Therapeutic potential of dietary bioactive compounds against anti-apoptotic Bcl-2 proteins in breast cancer. *Crit. Rev. Food Sci. Nutr.* **2025**, *65*, 4915-4940, https://doi.org/10.1080/10408398.2024.2398636.
10. Yadav, N.; Deshmukh, R.; Mazumder, R. A comprehensive review on the use of traditional Chinese medicine for cancer treatment. *Pharmacol. Res. Mod. Chin. Med.* **2024**, *11*, 100423, https://doi.org/10.1016/j.prmcm.2024.100423.
11. Xiang, Y.; Guo, Z.; Zhu, P.; Chen, J.; Huang, Y. Traditional Chinese medicine as a cancer treatment: Modern perspectives of ancient but advanced science. *Cancer Med.* **2019**, *8*, 1958-1975, https://doi.org/10.1002/cam4.2108.
12. Chunarkar-Patil, P.; Kaleem, M.; Mishra, R.; Ray, S.; Ahmad, A.; Verma, D.; Bhayye, S.; Dubey, R.; Singh, H.N.; Kumar, S. Anticancer Drug Discovery Based on Natural Products: From Computational Approaches to Clinical Studies. *Biomedicines* **2024**, *12*, 201, https://doi.org/10.3390/biomedicines12010201.
13. Kopustinskiene, D.M.; Jakstas, V.; Savickas, A.; Bernatoniene, J. Flavonoids as Anticancer Agents. *Nutrients* **2020**, *12*, 457, https://doi.org/10.3390/nu12020457.

14. Xu, Q.-X.; Wang, Z.-J.; He, Z.-C.; Xu, J.; Xu, W.; Yang, X.-W. Flavonoids dimers from the fruits of *Psoralea corylifolia* and their cytotoxicity against MCF-7 cells. *Bioorg. Chem.* **2023**, *130*, 106262, https://doi.org/10.1016/j.bioorg.2022.106262.
15. Murray, J.B.; Davidson, J.; Chen, I.; Davis, B.; Dokurno, P.; Graham, C.J.; Harris, R.; Jordan, A.; Matassova, N.; Pedder, C.; Ray, S.; Roughley, S.D.; Smith, J.; Walmsley, C.; Wang, Y.; Whitehead, N.; Williamson, D.S.; Casara, P.; Le Diguarher, T.; Hickman, J.; Stark, J.; Kotschy, A.; Geneste, O.; Hubbard, R.E. Establishing Drug Discovery and Identification of Hit Series for the Anti-apoptotic Proteins, Bcl-2 and Mcl-1. *ACS Omega* **2019**, *4*, 8892-8906, https://doi.org/10.1021/acsomega.9b00611.
16. Nguyen, H.D. Molecular docking and dynamic simulation of anti-apoptotic BCL-2 with saponins isolated from Weigela x "Bristol Ruby". *Indian J. Chem.* **2025**, *64*, 383-390, https://doi.org/10.56042/ijc.v64i4.15530.
17. Van Der Spoel, D.; Lindahl, E.; Hess, B.; Groenhof, G.; Mark, A.E.; Berendsen, H.J.C. GROMACS: Fast, flexible, and free. *J. Comput. Chem.* **2005**, *26*, 1701-1718, https://doi.org/10.1002/jcc.20291.
18. Guex, N.; Peitsch, M.C. SWISS-MODEL and the Swiss-Pdb Viewer: An environment for comparative protein modeling. *ELECTROPHORESIS* **1997**, *18*, 2714-2723, https://doi.org/10.1002/elps.1150181505.
19. Zoete, V.; Cuendet, M.A.; Grosdidier, A.; Michielin, O. SwissParam: A fast force field generation tool for small organic molecules. *J. Comput. Chem.* **2011**, *32*, 2359-2368, https://doi.org/10.1002/jcc.21816.
20. Pettersen, E.F.; Goddard, T.D.; Huang, C.C.; Couch, G.S.; Greenblatt, D.M.; Meng, E.C.; Ferrin, T.E. UCSF Chimera—A visualization system for exploratory research and analysis. *J. Comput. Chem.* **2004**, *25*, 1605-1612, https://doi.org/10.1002/jcc.20084.
21. Neese, F. Software Update: The ORCA Program System—Version 6.0. *WIREs Comput. Mol. Sci.* **2025**, *15*, e70019, https://doi.org/10.1002/wcms.70019.
22. Hanwell, M.D.; Curtis, D.E.; Lonie, D.C.; Vandermeersch, T.; Zurek, E.; Hutchison, G.R. Avogadro: an advanced semantic chemical editor, visualization, and analysis platform. *J. Cheminform.* **2012**, *4*, 17, https://doi.org/10.1186/1758-2946-4-17.
23. Knizia, G.; Klein, J.E.M.N. Electron Flow in Reaction Mechanisms—Revealed from First Principles. *Angew. Chem., Int. Ed.* **2015**, *54*, 5518-5522, https://doi.org/10.1002/anie.201410637.
24. Luo, J.; Xue, Z.Q.; Liu, W.M.; Wu, J.L.; Yang, Z.Q. Koopmans' Theorem for Large Molecular Systems within Density Functional Theory. *J. Phys. Chem. A* **2006**, *110*, 12005-12009, https://doi.org/10.1021/jp063669m.
25. Das, R.; Vigneresse, J.-L.; Chattaraj, P.K. Chemical reactivity through structure-stability landscape. *Int. J. Quantum Chem.* **2014**, *114*, 1421-1429, https://doi.org/10.1002/qua.24706.
26. Millan-Casarrubias, E.J.; García-Tejeda, Y.V.; González-De la Rosa, C.H.; Ruiz-Mazón, L.; Hernández-Rodríguez, Y.M.; Cigarroa-Mayorga, O.E. Molecular Docking and Pharmacological In Silico Evaluation of Camptothecin and Related Ligands as Promising HER2-Targeted Therapies for Breast Cancer. *Curr. Issues Mol. Biol.* **2025**, *47*, 193, https://doi.org/10.3390/cimb47030193.
27. Majewski, M.; Barril, X. Structural Stability Predicts the Binding Mode of Protein–Ligand Complexes. *J. Chem. Inf. Model.* **2020**, *60*, 1644-1651, https://doi.org/10.1021/acs.jcim.9b01062.

Publisher's Note & Disclaimer